

PAPER • OPEN ACCESS

Low-field magnetic anisotropy of Sr_2IrO_4

To cite this article: Muhammad Nauman *et al* 2022 *J. Phys.: Condens. Matter* **34** 135802

View the [article online](#) for updates and enhancements.

You may also like

- [Spectral functions of \$\text{Sr}_2\text{IrO}_4\$: theory versus experiment](#)
B Lenz, C Martins and S Biermann
- [Evolution of Oxygen Ligands upon Large Redox Swings of \$\text{Li}_3\text{IrO}_4\$](#)
Haifeng Li, Arnaud J. Pérez, Beata Taudul *et al.*
- [Decoupling of magnetism and electric transport in single-crystal \$\(\text{Sr}_{1-x}\text{A}_x\)_2\text{IrO}_4\$ \(A = Ca or Ba\)](#)
H D Zhao, J Terzic, H Zheng *et al.*




IOP | ebooks™

Bringing together innovative digital publishing with leading authors from the global scientific community.

Start exploring the collection—download the first chapter of every title for free.

Low-field magnetic anisotropy of Sr₂IrO₄

Muhammad Nauman^{1,2}, Tayyaba Hussain², Joonyoung Choi²,
Nara Lee³, Young Jai Choi³, Woun Kang⁴ and Younjung Jo^{2,*}

¹ Thermodynamics of Quantum Materials Laboratory, Institute of Science and Technology (IST) Austria, Klosterneuburg 3400, Austria

² Department of Physics, Kyungpook National University, Daegu 41566, Republic of Korea

³ Department of Physics, Yonsei University, Seoul 03722, Republic of Korea

⁴ Department of Physics, Ewha Womans University, Seoul 03760, Republic of Korea

E-mail: jophy@knu.ac.kr

Received 24 October 2021, revised 11 December 2021

Accepted for publication 5 January 2022

Published 20 January 2022



Abstract

Magnetic anisotropy in strontium iridate (Sr₂IrO₄) is essential because of its strong spin–orbit coupling and crystal field effect. In this paper, we present a detailed mapping of the out-of-plane (OOP) magnetic anisotropy in Sr₂IrO₄ for different sample orientations using torque magnetometry measurements in the low-magnetic-field region before the isospins are completely ordered. Dominant in-plane anisotropy was identified at low fields, confirming the *b* axis as an easy magnetization axis. Based on the fitting analysis of the strong uniaxial magnetic anisotropy, we observed that the main anisotropic effect arises from a spin–orbit-coupled magnetic exchange interaction affecting the OOP interaction. The effect of interlayer exchange interaction results in additional anisotropic terms owing to the tilting of the isospins. The results are relevant for understanding OOP magnetic anisotropy and provide a new way to analyze the effects of spin–orbit-coupling and interlayer magnetic exchange interactions. This study provides insight into the understanding of bulk magnetic, magnetotransport, and spintronic behavior on Sr₂IrO₄ for future studies.

Keywords: Sr₂IrO₄, torque measurement, magnetic anisotropy, spin–orbit-coupled magnetic exchange interaction

(Some figures may appear in colour only in the online journal)


1. Introduction

Currently, 5d transition metal oxides have emerged as a captivating class of materials arising from strong spin–orbit or electron–lattice interactions [1–3]. This strongly interacting many-body system provides a viable platform for studying unique frustrations and anisotropic magnetic interactions [4–7]. The strong spin–orbit coupling (SOC) in these materials makes them most suitable for high-temperature superconductors, topological insulators, and devices with spintronics functionality [8]. Recent advances have opened a new paradigm for achieving spintronic functionality, namely,

antiferromagnetic spintronics [1, 2, 4–6, 9–13]. Specifically, antiferromagnetic materials are of great interest because they have advantages such as no stray fields, insensitivity to magnetic fields, and fast antiferromagnetic (AFM) dynamics [14–17].

Strontium iridate (Sr₂IrO₄) is a representative of a 5d strongly correlated electronic system with a space group *I41/acd* [142]. In a free Ir atom, the 5d states are degenerated because of the rotational symmetry of the atomic Hamiltonian. However, the crystal field removes the degeneracy and splits the 5d orbital. The 5d states are split into high-energy two-fold-degenerate (*e_g*) states and low-energy three-fold-degenerate (*t_{2g}*) states. The total effective orbital angular momentum (*l_{eff}*) of the *t_{2g}* state is 1, and the total spin sums up to 1/2. Because a strong SOC essentially entangles the spin and orbital momenta, a unique *J_{eff}* = 1/2 quantum state is formed by the pure spins and spatially anisotropic orbitals.

* Author to whom any correspondence should be addressed.

 Original content from this work may be used under the terms of the [Creative Commons Attribution 4.0 licence](https://creativecommons.org/licenses/by/4.0/). Any further distribution of this work must maintain attribution to the author(s) and the title of the work, journal citation and DOI.

This novel $J_{\text{eff}} = 1/2$ state can provide a comprehensive understanding of the correlation between the anisotropic magnetoresistance and magnetocrystalline anisotropy and also help explore possible controllable AFM spintronics [16, 18–22]. Magnetic anisotropy is a key phenomenon driven by a strong electron correlation. Magnetic anisotropy interactions and anisotropy energy are used in several industrial and technical fields [23]. The magnetocrystalline anisotropy in antiferromagnets arises from relativistic SOC. Moreover, microscopic observations have shown that the first nearest-neighbor basal-plane exchange constant is higher (60 meV) than the interlayer exchange constant (1 μeV), indicating a strong magnetic anisotropy [15, 24, 25].

The $J_{\text{eff}} = 1/2$ isospins in Sr_2IrO_4 can be modulated by applying an external magnetic field [5, 15, 20, 26]. An in-plane canted AFM ordering arises below $T_N \sim 240$ K owing to the antisymmetric exchange interaction known as the Dzyaloshinskii–Moriya interaction (DMI) [27, 28]. DMI competes with the symmetric Heisenberg interaction and favors spin-canting in an otherwise AFM system. A spin-canting angle of $\sim 12^\circ$ results in a net magnetic moment in each domain. However, AFM ordering along the c axis leads to a zero net magnetization [29]. Moreover, the fascinating feature of Sr_2IrO_4 is that it exhibits both weak ferromagnetic (WFM) and AFM characteristics. The magnetic anisotropy and isospin reorientation substantially affect the electronic transport properties, making the material ideal for AFM-based spintronics functionality [20, 30, 31]. The magnetocrystalline contribution to the magnetic anisotropy in single-crystal Sr_2IrO_4 has been demonstrated based on torque magnetometry up to 9 T [3, 30]. Furthermore, a two-fold sawtooth shape of the out-of-plane (OOP) rotation torque was evaluated. This strong OOP magnetic anisotropy shows that the magnetic easy axis is along the in-plane direction. In addition, the field-induced WFM order is attributed only to the in-plane component of the external magnetic field. Thus, we conducted a detailed study on the in-plane magnetic anisotropy in single-crystal Sr_2IrO_4 and found the b axis to be the easy axis of magnetization [23]. However, there is a lack of mapping of the explicit evolution of the isospins and the magnetic anisotropy for different OOP rotations. Moreover, investigating the magnetic anisotropy of single-crystal Sr_2IrO_4 is essential, particularly in the low-magnetic-field region before the isospins are fully ordered.

Therefore, in this study, we verified OOP magnetic anisotropy before and after WFM transition and analyzed the ac and bc plane anisotropies separately. Here, we present a comprehensive study of the low-field isospin interactions that generate in-plane anisotropy, where the static magnetic-domain structure is related to the orientation of the magnetic easy axis. Because Sr_2IrO_4 is a layered material, we cannot ignore the interfacial anisotropy and interlayer exchange. Thus, this study considered the various factors contributing to the anisotropy, such as the shape, interfacial direction, interlayer exchange, and crystal symmetry, in the typical single-crystal Sr_2IrO_4 exhibiting strong SOC.

2. Materials and methods

Sr_2IrO_4 crystals were prepared using a flux method with SrCl_2 as the flux [3]. The crystallinity was confirmed using x-ray diffraction measurements. Single-crystal Sr_2IrO_4 was mounted on a piezoresistive cantilever with a crystallographic c axis perpendicular to the lever plane. The change in the torque was measured through the change in the resistance of the piezo material comprising a Wheatstone bridge circuit [3, 23]. This is a nondestructive and reliable technique for detecting spin canting and domain magnetization. The magnetic field direction with respect to the crystal axis was controlled using a rotator. Moreover, we applied the OOP angular-dependent torque of Sr_2IrO_4 , i.e., $\tau(\theta)$, for various crystal orientations by varying ψ . Here, θ is the angle between the applied magnetic field and the ab plane, and ψ is the crystal orientation with respect to the reference axis in the in-plane direction, see figure 1(a).

3. Results and discussion

Figure 1(b) shows the magnetization at 30 K when a magnetic field is applied along the ab plane. The magnetization gradually increases and saturates above a certain critical field at approximately 0.3 T with a small saturated moment [30]. A low degree of hysteresis with a negligible amount of residual net magnetization can be observed, indicating the WFM nature of Sr_2IrO_4 along the ab plane. Two distinguishable domains are present: one with isospins along the b axis and the other with isospins along the a axis. A correlation exists between the isospin direction and the stacking pattern, implying the presence of anisotropic interlayer coupling [30]. The regions can be divided into a low field (< 0.3 T) with a mixed-domain state and a high field (> 0.3 T) with the WFM state. Figure 1(c) shows the various crystal orientations with respect to the reference axis marked by a red dotted line. Note that ψ is a measure of the angle between the reference line and one specific corner of the crystal. A solid red line is displayed at one corner of the crystal to clarify the Ψ crystal orientation. Crystals usually grow in high symmetry direction and provide a clue regarding the crystallographic a and b axes. Based on the crystalline morphology of SIO, we designated one corner as the a axis, later confirmed after x-ray diffraction measurement. We performed the angle-dependent torque $\tau(\theta)$ at $\Psi = 0^\circ, 25^\circ, 90^\circ, 120^\circ$, and 180° . By comparing $\tau(\theta)$ at $\Psi = 0^\circ$ and 180° , as shown in figure 1(d), we determine whether there is a difference in the magnetization strengths along the positive and negative a axes in the basal plane. Identical $\tau(\theta)$ values for $\Psi = 0^\circ$ (solid line) and 180° (dotted line), including hysteresis around $\theta = 90^\circ$, are observed. This confirms that the crystal is accurately placed on the cantilever without torsion. The result represents the uniaxial magnetic behavior of the crystal along the in-plane direction. Hence, the two-fold torque curves come from the domain magnetization and AFM ordering in Sr_2IrO_4 . Furthermore, the

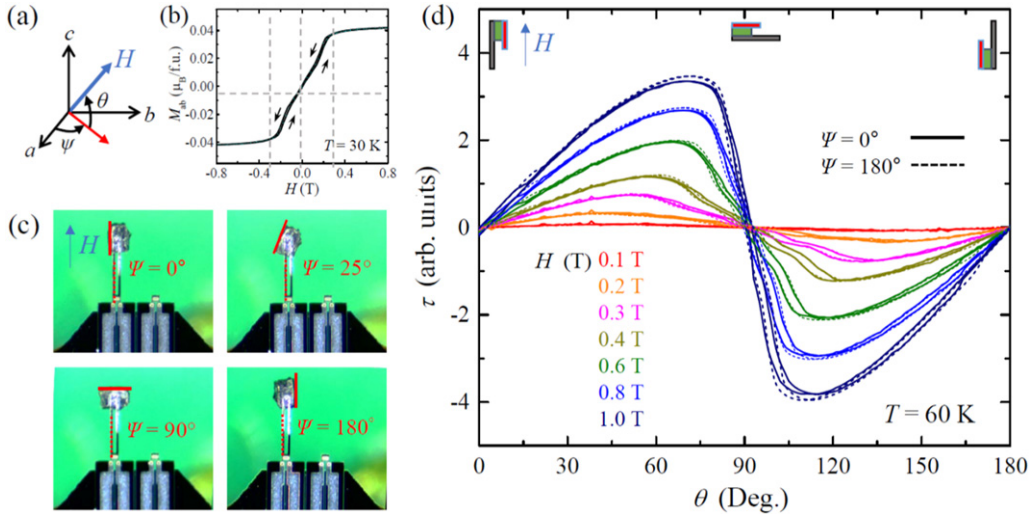


Figure 1. (a) Definition of θ and ψ angles. (b) Magnetization at 30 K under a magnetic field applied along the ab plane. (c) Images of the crystal placed on the cantilever adjusted to various ψ angles. ψ is a measure of the angle between the reference line marked with red dotted and solid lines at one crystal corner. (d) $\tau(\theta)$ values for two opposite directions along the a axis, i.e., $\psi = 0^\circ$ and 180° . The top sketch shows the alignment of the cantilever with the sample surface (red) parallel or perpendicular to the magnetic field.

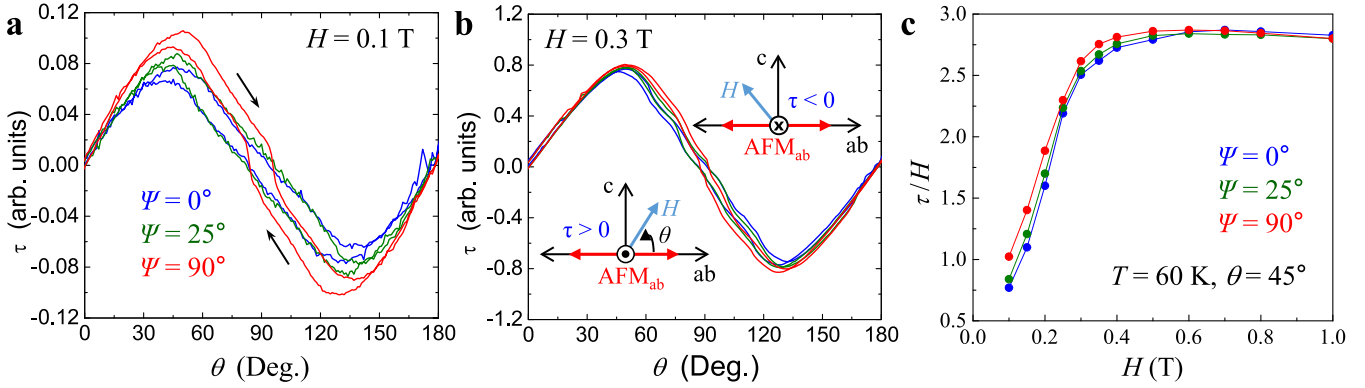


Figure 2. $\tau(\theta)$ values for three sample orientations ($\psi = 0^\circ, 25^\circ,$ and 90°) at (a) 0.1 T and (b) 0.3 T. (c) Amplitudes of the torque (τ/H) at $\theta = 45^\circ$ for different ψ values. Inset in (b) shows the sketch of negative and positive torque signals.

sawtooth response of the torque in high magnetic fields is a dominant characteristic of Sr_2IrO_4 with a strong SOC. $\tau(\theta)$ vanishes at $\theta = 0^\circ$ (180°) and $\theta = 90^\circ$, indicating that the easy axis is either parallel or perpendicular to the crystal surface. As θ increases, the gradually increasing torque changes rapidly in the opposite direction near $\theta = 90^\circ$, where the magnetic field passes through the c axis. This is characterized by a spin flop-like structure, indicating that the c axis is a hard magnetization axis and confirming the presence of an easy axis along the ab plane when the sample surface is parallel to the field direction, i.e., when $\theta = 0^\circ$ (180°). This coincides with the reported AFM alignment of magnetic-domain magnetization along the a axis [32].

Figures 2(a) and (b) shows the $\tau(\theta)$ values for $\Psi = 0^\circ$ (ac rotation), $\Psi = 90^\circ$ (bc rotation), and $\Psi = 25^\circ$ at $H = 0.1$ T and $H = 0.3$ T, respectively. At $H = 0.1$ T, the torque amplitude continuously increases when Ψ varies from 0° to 90° , which can be explained by the increase in the magnetization strength. This dominant in-plane anisotropy at a low field becomes isotropic at higher fields. The magnetic field-dependent

amplitude of τ/H at $\theta = 45^\circ$, shown in figure 2(c), represents the relative amplitude of the magnetization. The difference in the amplitudes for different Ψ values solely arises from the difference in the magnetization strengths along the a and b axes, given that the c axis magnetization is insignificant in Sr_2IrO_4 [30]. The hysteresis is significant in the low- H regime ($H < 0.3$ T), reported as canted AFM-domain states [23]. Moreover, the hysteresis disappears at 0.3 T, known as the field value where the WFM state is established [26, 30]. The jump-like trait approximately at $\theta = 90^\circ$ is prominent only under bc rotation ($\Psi = 90^\circ$). This difference in the torque curves might be due to the difference in the domain populations along the a and b axes.

Figure 3 shows the $\tau(\theta)$ values for $\Psi = 0^\circ$ under various magnetic fields at 60 K. The $\sin 2\theta$ angle dependence of the torque curves in the low- H regime is a characteristic of the linear response regime, while the deviation from this behavior at higher fields is direct evidence of the strong magnetic correlation. The sawtooth shape of the $\tau(\theta)$ curve at higher fields

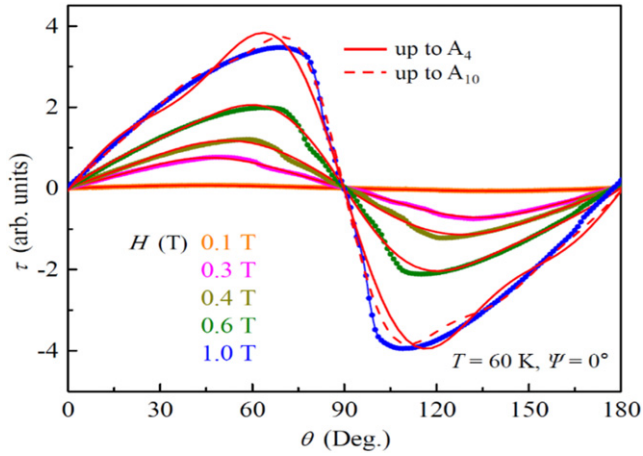


Figure 3. $\tau(\theta)$ values for $\psi = 0^\circ$ under various magnetic fields at 60 K. The solid red line represents the fitted model.

(>1 T) indicates the AFM ordering of the spins [3]. Generally, applying a high magnetic field overcoming all the magnetic correlations helps restore the $\sin 2\theta$ dependence due to the contribution of the Zeeman energy. However, in our case, the persistence of the sawtooth behavior above 0.3 T confirms the existence of a strong spin correlation [33].

To investigate the OOP magnetic anisotropies, we fitted the $\tau(\theta)$ curves. We introduced a mathematical model to determine the strong uniaxial magnetic anisotropy for multilayered systems [34]. Because of the layered structure of Sr_2IrO_4 , acting as a natural thin film, and electrons whose isospin orientation are strongly coupled to the pure spin magnetic moment in the plane, the model can be modified as follows:

The magnetic free energy can be written as $F = F_A + F_D + F_H$, which is the summation of the anisotropy energy (F_A), demagnetization energy (F_D), and free energy under an applied magnetic field (F_H), such that

$$F_A = k_1 \sin^2 \theta + k_2 \sin^4 \theta \quad (1a)$$

$$F_D = 2\pi M^2 \sin^2 \theta \quad (1b)$$

$$F_H = -MH \cos(\varphi - \theta) \quad (1c)$$

Here, k_1 and k_2 are the second-order uniaxial anisotropy terms, and θ and φ are the angles of the magnetic field (H) and magnetization axis (M) from the ab plane, respectively.

Reducing the total energy of the system under equilibrium conditions ($\frac{\partial F}{\partial \theta} = 0$) and rearranging the equations yield:

$$0 = (k_1 + k_2 + 2\pi M^2) \sin 2\theta - \frac{1}{2}k_2 \sin 4\theta - MH \sin(\varphi - \theta). \quad (2)$$

In equation (2), we set the coefficients of $\sin 2\theta$ and $\sin 4\theta$ as A_2 and A_4 , respectively. The third term corresponds to the torque (τ); therefore, τ becomes

$$\tau(\theta) = A_2 \sin 2\theta + A_4 \sin 4\theta. \quad (3)$$

A_2 characterizes an easy plane if $A_2 > 0$ and the easy axis if $A_2 < 0$. τ will be zero when $\varphi = \theta$, i.e., when H

and M are parallel. For Sr_2IrO_4 , the demagnetization energy contribution was negligible owing to the insignificant shape anisotropy [35]. Thus, extracting information regarding magnetic anisotropy is easy because of the crystal symmetry in the presence of H . The red solid lines in figure 3 indicate the fitting result obtained using equation (3). Up to 0.3 T, the fitting equation yields a relatively good fit. Nevertheless, the higher the magnetic field, the worse the fitting. To obtain a more accurate fitting curve, we added a higher-order anisotropy term to equation (3) as follows.

$$\tau = A_2 \sin 2\theta + A_4 \sin 4\theta + A_6 \sin 6\theta + A_8 \sin 8\theta + A_{10} \sin 10\theta. \quad (4)$$

The red dotted line indicates the fitting results on $\tau(\theta)$ at 1 T using equation (4). In this case, the result improves but still not perfect.

Anisotropic magnetism can be estimated by comparing the amplitude of the n th-fold symmetric contribution, A_n (see figure 4(a)). Two-fold symmetry contributions are the major contributions, as evident from the $\tau(\theta)$ curves. The amplitude of $\sin 2\theta$ (A_2) is positive at all magnetic fields, confirming that the anisotropy in Sr_2IrO_4 is an easy-plane type. A_2 is higher for $\Psi = 90^\circ$ than for $\Psi = 0^\circ$, indicating that the bc plane is an easy plane. A_2 gradually changes in the low- H regime and then increases linearly. This demonstrates the weak spin responses because of the lower Zeeman energy contributions in the low- H regime. The nonsaturation of all A_n up to 1 T is because the applied magnetic field is insufficient to overcome the high anisotropic energy barrier between the ab plane and the c axis. A_2 encodes all possible anisotropy contributions, including both intrinsic characteristics, such as the crystal structure and magnetic interaction, and extrinsic characteristics, such as the shape and surface effects. As reported in the literature, the extrinsic contributions are insignificant in Sr_2IrO_4 because of the small crystal dimensions (0.1 mm) and minor spin-glass phenomena [35]. The superexchange interaction between Ir moments in Sr_2IrO_4 is mediated by non-magnetic oxygen. The responsible strong SOC for microscopic antisymmetric exchange interaction, which competes with isotropic Heisenberg exchange, leads to a tilted Ir–O–Ir bond angle of 178° along the in-plane. Thus, the main anisotropic effect arises from a spin–orbit-coupled magnetic exchange interaction. The higher-order term is essential in systems exhibiting interfacial anisotropy. The 4_1 screw-axis symmetry about the c axis and strong SOC in Sr_2IrO_4 necessitates the inclusion of this interfacial anisotropy. In our OOP measurements of Sr_2IrO_4 , interfacial anisotropy cannot be a premise for total magnetic anisotropy; however, it is a prominent factor along with SOC in the OOP magnetic anisotropy. Thus, the main anisotropic effect arises from a spin–orbit-coupled magnetic exchange interaction. The higher-order term is essential in systems exhibiting interfacial anisotropy. This interfacial anisotropy is most common in magnetic thin films. In our OOP measurements of Sr_2IrO_4 , interfacial anisotropy cannot be a premise for total magnetic anisotropy; however, it cannot be excluded.

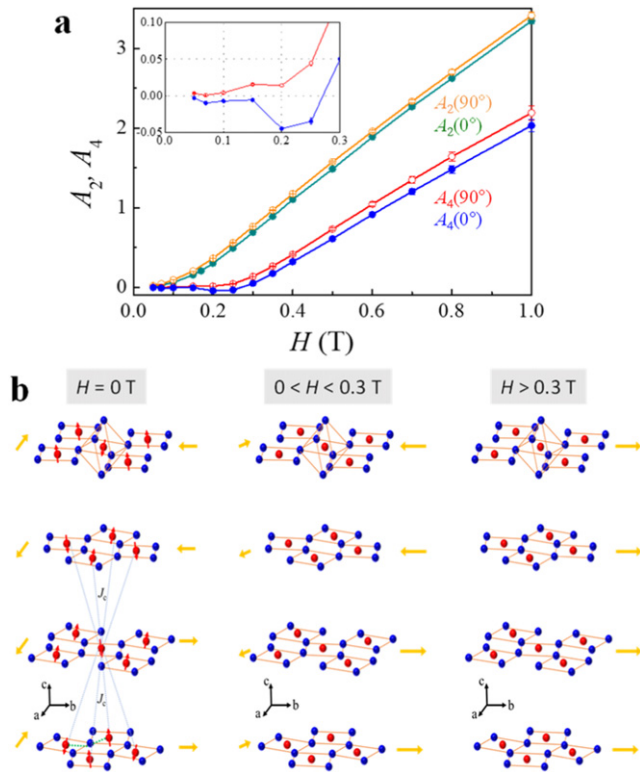


Figure 4. (a) Fitting parameters A_n ($n = 2, 4$) obtained using equation (3). (b) Stacking pattern of the canted AFM domain in Sr_2IrO_4 . Red arrows represent the magnetic moments carried by $J_{\text{eff}} = 1/2$ isospins. Yellow arrows to the left and right of each IrO_2 layer denotes the direction of net magnetic moments for AFM_a and AFM_b , respectively. Iridate octahedral shows one of the iridium ions in the top layer, whereas the green dashed line in the bottom layer shows a 178° Ir–O–Ir bond angle along the ab -plane. Light blue dotted lines represent the out-of-plane exchange interaction.

Nonzero A_4 appears near the high-field regime ($H > 0.3$ T) when $\tau(\theta)$ deviates from the $\sin 2\theta$ pattern. Since SIO has weak OOP magnetic coupling or magnetic exchange interaction [15, 32], nonzero A_4 pertains to the weakly coupled regions whose high prospect is in the OOP anisotropy measurements. In the low- H regime ($H < 0.3$ T), A_4 is negative for $\Psi = 0^\circ$ and positive for $\Psi = 90^\circ$, as shown in the inset of figure 4. The positive value of A_2 ($A_2 > 0$) and the negative value of A_4 ($A_4 < 0$) for $\Psi = 0^\circ$ (ac rotation) can be interpreted as the canted state, indicating AFM ordering along the a axis in the ab plane [32]. This result is also associated with a metamagnetic transition, where the system first becomes AFM_a (AFM ordering along the a axis) and then transitions to an FM state above 0.3 T by applying a magnetic field along the in-plane [36]. Because the b axis is an easy axis of magnetization, no such $A_4 < 0$ can be observed for $\Psi = 90^\circ$ (bc rotation) in the absence of any metamagnetic transition. Coupling along the c axis (J_c) is weaker than in-plane coupling (J_{ab}) [15]. As a correlation exists between the isospin direction and the stacking pattern, the anisotropic interlayer coupling is present depending on the field applied along the a axis or the b axis. An evolution of the domains with increasing applied magnetic field is shown in figure 4(b), where the system magnetizes along the easy b axis in a right–right–right–right pattern above

the critical field value >0.3 T. The shift toward positive values above 0.3 T is because the FM state cannot be realized by applying H along the hard axis, i.e., c axis. The application of a high field along the OOP direction will induce magnetization along the c axis owing to the tilting of the isospins. Such slight tilting of the isospins generates additional anisotropic terms (A_4 and higher-order parameters) and provides important information about the system. This will lead to the emergence of higher orders at fields >0.3 T, and off-diagonal interactions will lead to a sawtooth behavior in $\tau(\theta)$. The reason for the increase in the bifurcation of the A_4 curves for ac and bc rotations in the high-field regime remains unknown.

4. Conclusions

Based on torque magnetometry measurements of single-crystal Sr_2IrO_4 for different OOP rotations, we identified the in-plane magnetic anisotropy, which coincided with the AFM alignment of the magnetic domain along the a axis. This dominant in-plane anisotropy at low fields with a mixed-domain state becomes isotropic in higher fields with the WFM state. The sawtooth response of the torque in a high magnetic field is characterized by a spin flop-like change when the field passes through the c axis, which is a hard magnetization axis. The deviation from the $\sin 2\theta$ dependence of the torque is direct evidence of a strong magnetic correlation. By performing a fitting analysis of the strong uniaxial magnetic anisotropy, we compared the amplitudes of the two-fold (A_2) and four-fold (A_4) symmetric contributions. The higher value of A_2 for bc rotation than for ac rotation indicates that the bc plane is an easy plane. The nonzero value of A_4 in the high-field regime is attributed to a weakly coupled interlayer direction along with a slight tilting of the isospins generates additional anisotropic terms. Our results provide complete mapping of OOP magnetic anisotropy, verifying that the major anisotropic effects arise from spin–orbit-coupled magnetic exchange interactions. The results are relevant to understanding the giant magnetoresistance effect in a single crystal Sr_2IrO_4 reported recently [15]. This study provides insights into the OOP magnetic anisotropy in a low (<1 T) magnetic field regime.

Acknowledgments

YJ was supported by the National Research Foundation of Korea (NRF) (Grant Nos. NRF-2018K2A9A1A06069211 and NRF-2019R1A2C1089017). The work at Yonsei was supported by the NRF (Grant Nos. NRF-2017R1A5A-1014862 (SRC program: vdWMRC center), NRF-2019R1A2C2002601, and NRF-2021R1A2C1006375). WK acknowledges the support by the NRF (Grant Nos. 2018R1D1A1B07050087, 2018R1A6A1A03025340).

Data availability statement

All data that support the findings of this study are included within the article (and any supplementary files).

ORCID iDs

Muhammad Nauman  <https://orcid.org/0000-0002-2111-4846>

Young Jai Choi  <https://orcid.org/0000-0001-8030-583X>

Younjung Jo  <https://orcid.org/0000-0001-8030-583X>

References

- [1] Zwartsenberg B *et al* 2020 Spin–orbit-controlled metal–insulator transition in Sr₂IrO₄ *Nat. Phys.* **16** 290–4
- [2] Ye F, Hoffmann C, Tian W, Zhao H and Cao G 2020 Pseudospin-lattice coupling and electric control of the square-lattice iridate Sr₂IrO₄ *Phys. Rev. B* **102** 115120
- [3] Hong Y *et al* 2016 Large magnetic anisotropy in canted antiferromagnetic Sr₂IrO₄ single crystals *Phys. Rev. B* **93** 094406
- [4] Chen C *et al* 2020 Persistent insulating state at megabar pressures in strongly spin–orbit coupled Sr₂IrO₄ *Phys. Rev. B* **101** 144102
- [5] Bertinshaw J, Kim Y K, Khaliullin G and Kim B J 2019 Square lattice iridates *Annu. Rev. Condens. Matter Phys.* **10** 315–36
- [6] Souri M *et al* 2017 Optical signatures of spin–orbit exciton in bandwidth-controlled Sr₂IrO₄ epitaxial films via high-concentration Ca and Ba doping *Phys. Rev. B* **95** 235125
- [7] Kim B, Kim B H, Kim K and Min B I 2016 Substrate-tuning of correlated spin–orbit oxides revealed by optical conductivity calculations *Sci. Rep.* **6** 27095
- [8] Hermanns M, Kimchi I and Knolle J 2018 Physics of the Kitaev model: fractionalization, dynamic correlations, and material connections *Annu. Rev. Condens. Matter Phys.* **9** 17–33
- [9] Jackeli G and Khaliullin G 2009 Mott insulators in the strong spin–orbit coupling limit: from Heisenberg to a quantum compass and Kitaev models *Phys. Rev. Lett.* **102** 017205
- [10] Schaffer R, Kin-Ho Lee E, Yang B-J and Kim Y B 2016 Recent progress on correlated electron systems with strong spin–orbit coupling *Rep. Prog. Phys.* **79** 094504
- [11] Rau J G, Lee E K-H and Kee H-Y 2016 Spin–orbit physics giving rise to novel phases in correlated systems: iridates and related materials *Annu. Rev. Condens. Matter Phys.* **7** 195–221
- [12] Winter S M, Tsirlin A A, Daghofer M, van den Brink J, Singh Y, Gegenwart P and Valentí R 2017 Models and materials for generalized Kitaev magnetism *J. Phys.: Condens. Matter* **29** 493002
- [13] Natori W M H, Moessner R and Knolle J 2019 Orbital magnetic field effects in Mott insulators with strong spin–orbit coupling *Phys. Rev. B* **100** 144403
- [14] Maniv E *et al* 2021 Antiferromagnetic switching driven by the collective dynamics of a coexisting spin glass *Sci. Adv.* **7** eabd8452
- [15] Wang H, Lu C, Chen J, Liu Y, Yuan S L, Cheong S-W, Dong S and Liu J-M 2019 Giant anisotropic magnetoresistance and nonvolatile memory in canted antiferromagnet Sr₂IrO₄ *Nat. Commun.* **10** 2280
- [16] Zhou H, Xu Y-Y and Zhou S 2018 Electron correlations, spin–orbit coupling, and antiferromagnetic anisotropy in layered perovskite iridates Sr₂IrO₄ *Commun. Theor. Phys.* **70** 81
- [17] Nauman M *et al* 2021 Complete mapping of magnetic anisotropy for prototype Ising van der Waals FePS₃ *2D Mater.* **8** 035011
- [18] Louat A, Lenz B, Biermann S, Martins C, Bertran F, Le Fèvre P, Rault J E, Bert F and Brouet V 2019 ARPES study of orbital character, symmetry breaking, and pseudogaps in doped and pure Sr₂IrO₄ *Phys. Rev. B* **100** 205135
- [19] Khalyavin D D and Lovesey S W 2019 Anapole correlations in Sr₂IrO₄ defy the $j_{\text{eff}} = 1/2$ model *Phys. Rev. B* **100** 224415
- [20] Lu C and Liu J M 2019 The $J_{\text{eff}} = 1/2$ antiferromagnet Sr₂IrO₄: a Golden Avenue toward new physics and functions *Adv. Mater.* **32** 1904508
- [21] Calder S, Pajerowski D M, Stone M B and May A F 2018 Spin-gap and two-dimensional magnetic excitations in Sr₂IrO₄ *Phys. Rev. B* **98** 220402
- [22] Hussain T *et al* 2017 Pressure-induced metal–insulator transitions in chalcogenide NiS_{2-x}Se_x *Physica B* **536** 235
- [23] Nauman M, Hong Y, Hussain T, Seo M S, Park S Y, Lee N, Choi Y J, Kang W and Jo Y 2017 In-plane magnetic anisotropy in strontium iridate Sr₂IrO₄ *Phys. Rev. B* **96** 155102
- [24] Kim J *et al* 2012 Magnetic excitation spectra of Sr₂IrO₄ probed by resonant inelastic x-ray scattering: establishing links to cuprate superconductors *Phys. Rev. Lett.* **108** 177003
- [25] Fujiyama S, Ohsumi H, Komesu T, Matsuno J, Kim B J, Takata M, Arima T and Takagi H 2012 Two-dimensional Heisenberg behavior of $J_{\text{eff}} = 1/2$ isospins in the paramagnetic state of the spin-orbital Mott insulator Sr₂IrO₄ *Phys. Rev. Lett.* **108** 247212
- [26] Jeong J *et al* 2020 Magnetization density distribution of Sr₂IrO₄: deviation from a local $j_{\text{eff}} = 1/2$ picture *Phys. Rev. Lett.* **125** 097202
- [27] Kim J-W *et al* 2020 Controlling symmetry of spin–orbit entangled pseudospin state through uniaxial strain *Phys. Rev. B* **102** 054420
- [28] Liu P *et al* 2015 Anisotropic magnetic couplings and structure-driven canted to collinear transitions in Sr₂IrO₄ by magnetically constrained noncollinear DFT *Phys. Rev. B* **92** 054428
- [29] Samanta K *et al* 2020 Anisotropic lattice compression and pressure-induced electronic phase transitions in Sr₂IrO₄ *Phys. Rev. B* **101** 075121
- [30] Lee N, Ko E, Choi H Y, Hong Y J, Nauman M, Kang W, Choi H J, Choi Y J and Jo Y 2018 Antiferromagnet-based spintronic functionality by controlling isospin domains in a layered perovskite iridate *Adv. Mater.* **30** 1805564
- [31] Meyers D *et al* 2019 Magnetism in iridate heterostructures leveraged by structural distortions *Sci. Rep.* **9** 4263
- [32] Porras J *et al* 2019 Pseudospin-lattice coupling in the spin–orbit Mott insulator Sr₂IrO₄ *Phys. Rev. B* **99** 085125
- [33] Modic K A *et al* 2017 Robust spin correlations at high magnetic fields in the harmonic honeycomb iridates *Nat. Commun.* **8** 1–5
- [34] Pouloupoulos P, Flevaris N K, Krishnan R and Porte M 1994 Methods of determining magnetization and uniaxial anisotropy of multilayers by means of torque magnetometry *J. Appl. Phys.* **75** 4109–13
- [35] Fruchter L, Colson D and Brouet V 2016 Magnetic critical properties and basal-plane anisotropy of Sr₂IrO₄ *J. Phys.: Condens. Matter* **28** 126003
- [36] Zhang H *et al* 2020 Comprehensive electrical control of metamagnetic transition of a quasi-2D antiferromagnet by *in situ* anisotropic strain *Adv. Mater.* **32** 2002451